PAMM · Proc. Appl. Math. Mech. **17**, 95 – 98 (2017) / **DOI** 10.1002/pamm.201710028

Modelling of hydraulic fracturing and fluid flow change in saturated porous domains

Yousef Heider[1,*] and **Bernd Markert**[1]

[1] Institute of General Mechanics, RWTH Aachen University. Templergraben 64, 52062, Aachen, Germany

The underlying research work aims to develop a numerical model of pressure-driven fracturing of saturated porous media. This is based on the combination of the phase-field modelling (PFM) scheme together with a continuum-mechanical approach of multi-phase materials. The proposed modelling framework accounts for the crack nucleation and propagation in the solid matrix of the porous material, as well as the fluid flow change in the cracked region. The macroscopic description of the saturated porous material is based on the theory of porous media (TPM), where the proposed scheme assumes a steady-state behaviour (quasi-static) and neglects all thermal and chemical effects. Additionally, it assumes an open system with possible fluid mass production from external source. Special focus is laid on the description of the interface and change of the volume fractions and the permeability parameter between the porous domain and the crack. Finally, a numerical example using the finite element method is presented and compared with experimental data to show the ability of the proposed modelling strategy in capturing the basic features of hydraulic fracturing.

1 Introduction

Hydraulic fracturing is a very important subject in various engineering applications, especially in the energy sector, such as in geothermal applications, mining and petroleum. In the field of enhanced geothermal systems (EGS), which are applied to generate geothermal electricity through hot water, high-pressure water is injected into deep rock layers with low permeability in order to enhance the rock's permeability. This leads to improving the system's efficiency and helping to produce electricity with lower prices. Hydraulic fracturing using pressurised liquids with chemical additives is also used in petroleum engineering to extract shale gas. In a similar fashion, the developed numerical tools can be applied to simulate phenomena like intervertebral disc herniation in biomechanics.

The development of the phase-field modelling (PFM) of fracture can be traced back to Griffith [1], who described in 1921 the fracturing of brittle solids using elastic-energy-based mathematical formulations, where a critical energy release rate has been defined to start crack propagation. This criterion for the initiation of cracks has been later extended by Irwin [2], by introducing the strain-energy release rate and the fracture toughness concepts. The challenge in the numerical implementation of those approaches using, e.g., the finite element method, is the consideration of the cracks as discontinuities inside the continuous solid domain. Thus, the PFM has been introduced to tackle this problem, which approximates the sharp edges of the crack by a diffusive interface using a scalar field variable, called the phase-field variable. Therefore, no discontinuities in the geometry or the finite-element mesh takes place. Additionally, the PFM introduces an internal length scale parameter to define the width of the diffusive edge of the crack.

Apart from fracture mechanics, the idea of diffuse interfaces is found in physics, where it has been used by, e. g., Cahn and Hilliard [3] in 1958 to describe the interfaces in a heterogeneous system by a fourth-order partial differential equation. The link between the PFM and fracture mechanics, also within a variational framework, is found in later scientific works, such as in [4–8], allowing to model multi-dimensional, mixed-mode fracturing. Moreover, to estimate and study the physical meaning of the PFM parameters, a recent comparison between molecular dynamics (MD) simulations of fracture on the nano-scale and the continuum PFM scheme is found in [9].

The PFM has been later implemented to modelling of hydraulic fracturing in porous materials, induced by the increase of the pore pressure, see [10–15]. This leads, however, to permanent changes of the local physics of the problem, such as of the volume fractions and the permeability, which are discussed in more details in the following sections.

For the description of the behaviour of porous materials on a macroscopic scale, the theory of porous media (TPM) is applied [16, 17]. This mathematical model is based on the assumptions of a materially incompressible solid but compressible fluid, a quasi-static behaviour, no thermal or chemical effects or any mass exchange between the phases. However, the formulation allows for an external supply of the fluid phase, as will be shown in the numerical examples.

* Corresponding author: e-mail heider@iam.rwth-aachen.de, phone +49 241 80 98286, fax +49 241 80 92231

2 Mathematical modelling

The material under consideration is a two-phase porous material φ consisting of immiscible constituents φ^α ($\alpha = S$: solid, $\alpha = F$: fluid). Following the theory of porous media (TPM) [16], homogenisation is applied to a representative volume element (RVE), where the constituents are assumed to be in a state of ideal disarrangement. Thus, having the partial and total volume elements $\mathrm{d}v^\alpha$ and $\mathrm{d}v$, as well as the partial and material densities ρ^α and $\rho^{\alpha R}$, the volume fractions, the saturation condition and the density dependencies, respectively, read

$$n^\alpha := \mathrm{d}v^\alpha / \mathrm{d}v\,, \quad n^S + n^F = 1\,, \quad \rho^\alpha = n^\alpha \rho^{\alpha R}\,. \tag{1}$$

The solid phase incompressibility is associated with $\rho^{SR} = \text{const.}$. However, the pore fluid is considered compressible, and consists of a mixture of an incompressible liquid phase φ^L ($\rho^{LR} = \text{const.}$) and trapped, compressible, ideal gas bubbles φ^G [18, 19]. This behaviour is governed by the following relations:

$$n^F = n^L + n^G\,, \quad \rho^F = n^F \rho^{FR}(p) = n^L \rho^{LR} + n^G \rho^{GR}(p)\,, \quad \rho^{GR} = \frac{M}{R\,\Theta}\,p \longrightarrow \rho^{FR}(p) \approx \alpha_F + \beta_F\,(p - p_a)\,. \tag{2}$$

Herein, Eq. $(2)_3$ represents the ideal gas law, where p is the pore pressure with initial value equals to the atmospheric pressure p_a. R is the universal gas constant, $\Theta = \text{const.}$ is the absolute Kelvin's temperature and M is the molar mass of the gas. Applying linearisation to ρ^{FR} for simplicity results in a linear dependency of ρ^{FR} on p via the constants α_F, β_F, which can be determined based on the initial conditions. Concerning the kinematics, the motion of φ^S is characterised by a Lagrangean description via the solid displacement $\mathbf{u}_S$ and velocity $\mathbf{v}_S$. The pore-fluid flow is expressed in Eulerian settings using the fluid velocity $\mathbf{v}_F$, leading to the seepage velocity definition as $\mathbf{w}_F = \mathbf{v}_F - \mathbf{v}_S$. Within a geometrically linear framework, the linearised solid strain $\boldsymbol{\varepsilon}_S$ in Eq. $(3)_1$ is considered. Moreover, for the purely mechanical model, the partial mass balance Eq. $(3)_2$ and the partial momentum balance Eq. $(3)_3$ are employed:

$$\boldsymbol{\varepsilon}_S := \tfrac{1}{2}\,(\operatorname{grad}\,\mathbf{u}_S + \operatorname{grad}^T \mathbf{u}_S)\,, \quad (\rho^\alpha)'_\alpha + \rho^\alpha \operatorname{div}\mathbf{v}_\alpha = \hat{\rho}^\alpha\,, \quad \mathbf{0} = \operatorname{div}\boldsymbol{\sigma}^\alpha + \rho^\alpha\,\mathbf{b} + \hat{\mathbf{p}}^\alpha\,. \tag{3}$$

In this, $\hat{\rho}^\alpha$ is the mass supply term, which considers only the possible external fluid mass supply $\hat{\rho}^{Ext}$, as the mass exchange between the constituents is excluded. $\boldsymbol{\sigma}^\alpha$ is the symmetric partial Cauchy stress, $\mathbf{b}$ is the mass-specific body force acting on φ, and $\hat{\mathbf{p}}^\alpha$ denotes the direct local interaction force between φ^S and φ^F, where $\hat{\mathbf{p}}^S + \hat{\mathbf{p}}^F = \mathbf{0}$ must hold.
The hydraulic fracturing of saturated porous materials is modelled within the PFM approach, see, e.g. [4, 7, 10–12, 14]. Under the assumption of brittle fracture and following Griffith's definition, the global potential energy function $\mathcal{F}$ of a cracked linear-elastic, isotropic and homogenised porous body can be expressed as the sum of the elastic strain energy Ψ^S_{el} integrated over the whole domain and the critical fracture energy (Griffith's energy) G_c integrated over the crack surface as given in Eq. $(4)_1$. Introduction of the phenomenological phase-field variable d^S to distinguish between the cracked ($d^S = 1$) and the intact ($d^S = 0$) states of the material allows to transfer $\mathcal{F}$ into pure volume integral:

$$\mathcal{F}(\boldsymbol{\varepsilon}_S, \Gamma_c) = \int_\Omega \overline{\Psi}^S_{\text{el}}(\boldsymbol{\varepsilon}_S)\,\mathrm{d}v + \int_{\Gamma_c} G_c\,\mathrm{d}\Gamma_c\,, \quad \Longrightarrow \quad \mathcal{F}(\boldsymbol{\varepsilon}_S, d^S, \nabla d^S) = \int_\Omega \Big[\Psi^S_{\text{el}}(\boldsymbol{\varepsilon}_S, d^S) + \Psi^S_{\text{crack}}(d^S, \nabla d^S)\Big]\mathrm{d}v\,, \tag{4}$$

where $\Psi := \Psi^S_{\text{crack}} + \Psi^S_{\text{el}}$ and the fracture and elastic energies read:

$$\Psi^S_{\text{crack}}(d^S, \nabla d^S) = 2\,\psi_c\Big[(d^S) + \frac{\epsilon^2}{2}\,|\nabla d^S|^2\Big]\,, \quad \Psi^S_{\text{el}} = g(d^S)\Big[\frac{1}{2}\kappa^S\big[\mathrm{tr}^+(\boldsymbol{\varepsilon}_S)\big]^2 + \mu^S \boldsymbol{\varepsilon}^D_S \cdot \boldsymbol{\varepsilon}^D_S\Big] + \frac{1}{2}\kappa^S\big[\mathrm{tr}^-(\boldsymbol{\varepsilon}_S)\big]^2. \tag{5}$$

In this, ψ_c is a specific fracture energy per unit volume, introduced in [14] as a modification to G_c criterion in the crack energy formulation and based on gradient-damage mechanics. The aim of introducing ψ_c is to enforce the crack driving force to be zero as long as the occurring principal stresses are below a certain threshold σ^S_c (called the critical fracture stress). Moreover, ϵ is an internal length related to the crack transition zone and $g(d^S)$ is a degradation function given in terms of the residual stiffness η^S as $g(d^S) := (1 - \eta^S)(1 - d^S)^2 + \eta^S$. Additionally, $\kappa^S := \mu^S + (2/3)\lambda^S$ is the bulk modulus of the porous solid matrix and λ^S, μ^S are the Lamé parameters. $\boldsymbol{\varepsilon}^D_S$ is the elastic deviatoric strain tensor and $\mathrm{tr}\,(\boldsymbol{\varepsilon}_S) := \boldsymbol{\varepsilon}_S \cdot \mathbf{I} = \operatorname{div}\mathbf{u}_S$ is the trace of $\boldsymbol{\varepsilon}_S$ with $\mathrm{tr}^+(\boldsymbol{\varepsilon}_S) := \max\{0, \mathrm{tr}\,(\boldsymbol{\varepsilon}_S)\}$ and $\mathrm{tr}^-(\boldsymbol{\varepsilon}_S) := \min\{0, \mathrm{tr}\,(\boldsymbol{\varepsilon}_S)\}$ are the positive (tension) and the negative (compression) parts of the trace. Following the standard Ginzburg–Landau approach for the phase-field evolution, and considering quasi-static conditions, the phase-field equation reads

$$\frac{\partial \Psi}{\partial d^S} = 0 \quad \Longrightarrow \quad \underbrace{(1 - d^S)\,\tilde{\mathcal{D}}_c}_{\text{driving force}} = \underbrace{\Big[d^S - \epsilon^2 \Delta d^S\Big]}_{\text{geometric resistance}} \quad \text{with} \quad \tilde{\mathcal{D}}_c = \max_{\tau \in [0,t]} \Big\langle \sum_{i=1}^{3} \Big(\frac{\langle \overline{\sigma}^S_E \rangle_+}{\sigma^S_c}\Big)^2 - 1 \Big\rangle_+\,. \tag{6}$$

In this, $\langle(\,\bullet\,)\rangle_+ = \frac{1}{2}\big[(\,\bullet\,) + |(\,\bullet\,)|\big]$ represents the Macauley brackets, and we introduce $\overline{\sigma}^S_E := \frac{1}{3}\,\mathrm{tr}\,\boldsymbol{\sigma}^S_E$ as the volumetric part of the effective principal stresses under tension of the undamaged solid phase. The effective stress tensor in the momentum balance equation is derived as follows:

$$\boldsymbol{\sigma}^S_E = \frac{\partial \Psi^S_{\text{el}}(\boldsymbol{\varepsilon}_S, d^S)}{\partial \boldsymbol{\varepsilon}_S} = g(d^S)\Big[\kappa^S\,\mathrm{tr}^+(\boldsymbol{\varepsilon}_S)\,\mathbf{I} + 2\,\mu^S\,\boldsymbol{\varepsilon}^D_S\Big] + \kappa^S\,\mathrm{tr}^-(\boldsymbol{\varepsilon}_S)\,\mathbf{I}\,. \tag{7}$$

In the presence of the fracture, the volume fraction of φ^S and the intrinsic permeability tensor $\mathbf{K}^S$ are expressed as functions of d^S:

$$n^S = (1-d^S)\, n^S_{0S}\, (1-\operatorname{div}\mathbf{u}_S)\,, \quad K^S = \alpha_{\mathbf{u}}\, K^S_0 + \chi_d\, K^S_d \quad \text{with} \quad \alpha_{\mathbf{u}} = \left(\frac{n^F\, n^S_{0S}}{n^F_{0S}\, n^S}\right)^z \quad \text{and} \quad K^S_d = \frac{w_c^2}{12}\,, \tag{8}$$

where K^S_0 represents the initial permeability, K^S_d is the permeability in the crack and w_c is the crack width. The boundary indicator function $\chi_d := d^S$ if $d^S > 0.5$ and $\chi_d = 0$ if $d^S \leq 0.5$. The function $\alpha_{\mathbf{u}}$ with the parameter $z \geq 0$ controls the deformation dependency of the permeability, where $\alpha_{\mathbf{u}} = 1$ for $\chi_d := 0$.
In summary, the governing balance equations to solve initial-boundary-value problems (IBVPs) of brittle fracture with primary variables $\{\mathbf{u}_S, \mathbf{v}_F, p, d^S\}$ are in strong form Eq. (6) beside the following three equations:

$$\begin{aligned}
&\text{Overall momentum balance:} && \mathbf{0} = \operatorname{div}\left[\boldsymbol{\sigma}^S_E(\mathbf{u}_S\,,\phi^S) + \boldsymbol{\sigma}^F_E(\mathbf{v}_F) - p\,\mathbf{I}\right] + \rho\,\mathbf{b}\,,\\
&\text{Fluid Momentum balance:} && \mathbf{0} = \operatorname{div}\left[\boldsymbol{\sigma}^F_E(\mathbf{v}_F)\right] - n^F \operatorname{grad} p + \rho^F\,\mathbf{b} - (1-d^S)(n^F)^2\,\mu^{FR}\,(K^S)^{-1}\,\mathbf{w}_F\,,\\
&\text{Fluid mass balance:} && M_{sp}\, n^F \beta_F(p)'_S + \rho^{FR} \operatorname{div}\mathbf{v}_S - \operatorname{div}\left(\rho^{FR}\tfrac{K^S}{\mu^{FR}}(\operatorname{grad} p - \rho^{FR}\,\mathbf{b})\right) = \mathcal{Q}(\mathbf{x})\,\hat{\rho}^{Ext}\,.
\end{aligned} \tag{9}$$

Herein, $\boldsymbol{\sigma}^F_E = \mu^F(\operatorname{grad}\mathbf{v}_F + \operatorname{grad}^T\mathbf{v}_F)$ is the fluid effective stress, with $\mu^F := n^F\,\mu^{FR} > 0$ as the fluid dynamic viscosity. $\mathcal{Q}(\mathbf{x})$ is the source location function ($\mathcal{Q} = 1$ for the source and 0 otherwise). Equation $(9)_3$ results from insertion of the term $n^F\mathbf{w}_F$ from the fluid moment balance in the fluid mass balance equation, where the higher-order term $\operatorname{div}\operatorname{div}(\boldsymbol{\sigma}^F_E)$ is neglected. Moreover, we add a correction factor $M_{sp} > 1$ to the compressibility of fluid to fit with the experimental results. This considers the extra compressibility coming from the pressing pump and tubes as well as that due to the fact that the amount of fluid in the experiment is very much more than that of simulation. Finally, it is worth mentioning that the crack healing is prevented by applying the condition that the crack driving force $\tilde{\mathcal{D}}_c$ can only increase.

3 Numerical results and discussion

In the following, modelling of hydraulic fracturing of a Granite rock sample (300 x 300 x 450 mm^3) is presented. To mention some material properties, the initial solidity $n^S_{0S} = 0.99$, the initial permeability $K^S_0 = 10^{-19}\,\mathrm{m}^2$, Young's modulus $E^S = 85.5 \cdot 10^3$ MPa, Possion's ratio $\nu^S = 0.3$ and the effective solid density $\rho^{SR} = 2940$ kg/m^3. For simplicity, this experiment is modelled as a two-dimensional, plane-strain, linear elastic problem (see Fig. 1). The initial-boundary-value problem (IBVP) is subjected to the illustrated confining stresses and to an initial atmospheric pressure $p_a = 0.1$ MPa . In the centre of the sample, the fluid (highly viscous glycerol with effective viscosity $\mu^{FR} = 1.5\,\mathrm{N\,s\,/\,m^2}$) is injected with varying injection rate until onset of the crack, and then the injection is stopped. In the model, the critical fracture stress $\sigma^S_c = 13.8$ MPa and the internal length scale $\epsilon = 0.004$ m.
The progress of the crack, indicated by the phase-field variable, is illustrated in Fig. 2 . The crack propagates perpendicular to the maximum principal stress, which agrees with the observations of the experiments. Moreover, the time history of the pressure p at the centre of the sample is depicted in Fig. 3, which agrees also with the experiment as the compressible fluid starts relaxing after onset of the crack.

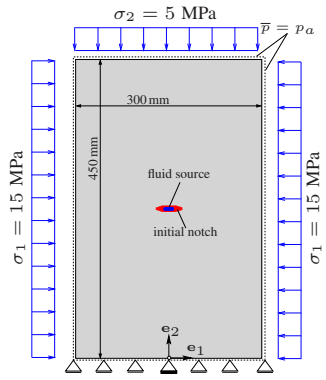

Fig. 1: Geometry and boundary conditions of the symmetric IBVP.

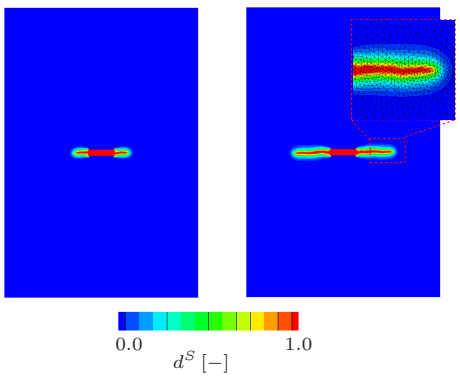

Fig. 2: Phase-field contour plots during crack propagation, and illustration of the fine mesh at the crack path.

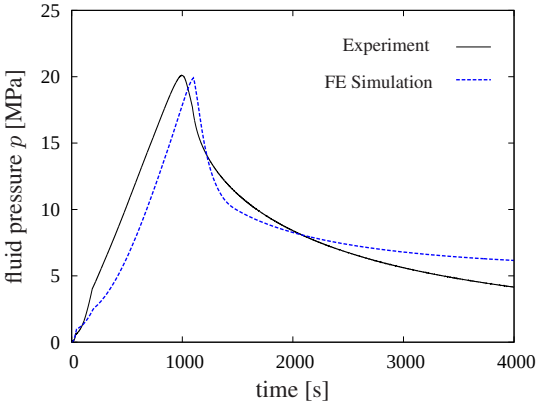

Fig. 3: Fluid pressure time history at the centre of the sample.

In conclusion, this study presented a robust macroscopic phase-field modelling approach of porous media hydraulic fracture, which can be implemented in usual finite element codes. A good agreement has been obtained between the experimental and the numerical results. To mention two aspects, as an example, the crack propagates in the 2D settings perpendicular to the

maximum principal stress, and the fluid pressure decreases in coincidence with the crack occurrence and propagation. This work, however, remains to have improvement areas and extensions, such as the description of the material heterogeneity and the extension towards efficient 3D simulations.

Acknowledgement: The authors would like to aknowlege the support of the Chair of Geotechnical Engineering and the Institute for Applied Geophysics and Geothermal Energy, E.ON Energy Research Center, RWTH Aachen University for providing the experimental data, which are related to the BMWi-Project 0325167.

References

[1] A. A. Griffith, Phil. Trans. Roy. Soc. Lond. **A 221**, 163–198 (1921).
[2] G. R. Irwin, J. Appl. Mech. **24**, 361–364 (1957).
[3] J. W. Cahn, J. E. Hilliard, J. Chem. Phys. **28**, 258–267 (1958).
[4] G. Francfort, J.-J. Marigo, J. Mechan. and Phys. Solids. **46**, 1319–1342 (1998).
[5] B. Bourdin, G. Francfort, J.-J. Marigo, J. Mech. Phys. Solids, **48**, 797–826 (2000).
[6] C. Kuhn, R. Müller, Eng. Fract. Mech. **77**, 3625–3634 (2010).
[7] C. Miehe, F. Welschinger, M. Hofacker, Int. J. Numer. Meth. Eng. **83**, 1273–1311 (2010).
[8] M. Ambati, T. Gerasimov, L. De Lorenzis, Comp. Mech. **55**, 383–405 (2015).
[9] S. P. Patil, Y. Heider, C. Hernandez-Padilla, E. Cruz-Chú, B. Markert, Comput. Methods Appl. Mech. Engrg. **312 (8)**, 117–129 (2016).
[10] B. Markert, Y. Heider, in: Recent Trends in Computational Engineering - CE2014, edited by M. Mehl, M. Bischoff, M. Schäfer, ISBN 978-3-319-22997-3 (Springer International Publishing, 2015), pp. 167–180.
[11] Y. Heider, B. Markert, Mech. Res. Commun. **80**, 38–46 (2017).
[12] A. Mikelić, M. F. Wheeler, T. Wick, Multiscale Model. Simul. **13**, 367–398 (2015).
[13] S. Lee, A. Mikelić, M. F. Wheeler, T. Wick, Comput. Methods Appl. Mech. Engrg. doi:10.1016/j.cma.2016.02.008.
[14] C. Miehe, S. Mauthe, Comput. Methods Appl. Mech. Engrg. **304**, 619–655 (2016).
[15] W. Ehlers, C. Luo, Comput. Methods Appl. Mech. Engrg. **315**, 348–368 (2017).
[16] W. Ehlers, in: Porous Media: Theory Experiments and Numerical Applications, edited by W. Ehlers, J. Bluhm, ISBN 3-540-43763-0 (Springer-Verlag, Berlin Heidelberg, 2002), pp. 3–86.
[17] B. Markert, Y. Heider, W. Ehlers, Int. J. Numer. Meth. Eng. **82**, 1341–1383 (2010).
[18] D. Mahnkopf, Institute of Applied Mechanics, University of Stuttgart, Report No. II-5 (2000).
[19] M. Schanz, S. Diebels, Acta Mech. **161**, 213–235 (2003).

